EuPA Open Proteomics 8 (2015) 85–93

Contents lists available at ScienceDirect

EuPA Open Proteomics

journal homepage: www.elsevier.com/locate/euprot

The proteomic landscape of glioma stem-like cells

Cheryl F. Lichti[a,b,*], Norelle C. Wildburger[a,c], Alexander S. Shavkunov[a], Ekaterina Mostovenko[a], Huiling Liu[a], Erik P. Sulman[d], Carol L. Nilsson[a,b]

[a] Department of Pharmacology & Toxicology, University of Texas Medical Branch, 301 University Blvd, Galveston, TX 77555-0617, United States
[b] UTMB Cancer Center, University of Texas Medical Branch, 301 University Blvd, Galveston, TX 77555-1074, United States
[c] Neuroscience Graduate Program, Graduate School of Biomedical Sciences, University of Texas Medical Branch, 301 University Blvd, Galveston, TX 77555-1074, United States
[d] Department of Radiation Oncology, The University of Texas M.D. Anderson Cancer Center, 1515 Holcombe Boulevard, Houston, TX 77030, United States

ARTICLE INFO

Article history:
Received 27 February 2015
Received in revised form 26 June 2015
Accepted 29 June 2015
Available online 17 July 2015

Keywords:
Glioblastoma
Glioma stem cells
Label-free quantitative proteomics
Ingenuity Pathway Analysis
DAVID
Unsupervised hierarchical clustering

ABSTRACT

Glioma stem-like cells (GSCs) are hypothesized to provide a repository of cells in tumors that can self-replicate and are radio- and chemo-resistant. GSC lines, representing several glioma subtypes, have been isolated and characterized at the transcript level. We sought to characterize 35 GSC lines at the protein level using label-free quantitative proteomics. Resulting relative fold changes were used to drive unsupervised hierarchical clustering for the purpose of classifying the cell lines based on proteomic profiles. Bioinformatics analysis identified synoviolin, serine/arginine-rich splicing factor 2, symplekin, and IL-5 as molecules of interest in progression and/or treatment of glioma.

1. Introduction

Primary brain tumors comprise 3% of all cancer diagnoses, and of these, GBM [World Health Organization (WHO) grade IV astrocytoma] makes up over half (52%) of all cases [1,2]. Despite an aggressive therapeutic regimen including surgical resection followed by some combination of chemotherapy and radiotherapy, the disease is ultimately fatal, with median survival only slightly over a year after diagnosis [2–6]. A deeper molecular-level understanding of the origins of GBM is critical in the quest to discover new therapeutic targets for this disease that few survive.

One factor that contributes to poor clinical outcome is the presence of a small subpopulation (<1%) of cells within the tumor which are both radio- and chemotherapy resistant [7–11]. These cells, termed glioma stem cells or glioma stem-like cells (GSCs) are postulated to provide a repository of cells for tumor recurrence [7–11]. GBM has been classified into several subgroups based upon patterns of gene expression [12–16], and this same classification scheme may be applied to GSCs. According to The Cancer Genome Atlas (TCGA), the GBM subgroups are classical, proneural, and mesenchymal [12–16]. Tumors themselves are not homogeneous; a recent study of biopsy samples revealed that cells from different regions of the same tumor show different molecular phenotypes [17]. Therefore, it is critical to understand GSCs at a molecular level in order to design an effective treatment regimen for GBM.

The purpose of our study was to perform a proteomic comparison of 35 GSCs, derived from patient tumors, in order to gain a deeper understanding of protein-level changes associated with GSCs and to identify potential therapeutic targets. The origin of GSCs has yet to be definitively determined, although glioma may originate from neural stem cells [18–22], glial cells [23], oligodendrocyte precursor cells [24], neurons [25] or astrocytes [25,26]. Given the difficulty in identifying an appropriate control for GSCs, each cell line was quantified relative to a mixed control sample containing an equal amount of protein from each cell line. The Catalog of Somatic Mutations in Cancer (COSMIC) database [27–31] was queried in order to compare our results with genome-level studies of patient tumor samples, especially for those proteins with no previous association to GBM. A combination of the Database for Annotation, Visualization and Integrated Discovery (DAVID) webtool [32,33] and Ingenuity Pathway Analysis (IPA) was used to determine affected pathways for each cell line, and IPA was used to determine predicted upstream regulators. Unsupervised hierarchical clustering of proteins and of upstream regulators was used to determine similar

* Corresponding author. Department of Pharmacology & Toxicology, University of Texas Medical Branch, 301 University Blvd, Galveston, TX 77555-0617, United States.
E-mail address: cflichti@utmb.edu (C.F. Lichti).

http://dx.doi.org/10.1016/j.euprot.2015.06.008

behavior between the cell lines. We identified symplekin (SYMPK) as a protein whose expression is significantly changed across several of our cell lines [34]. In addition, we identified novel putative upstream regulators interleukin-5 (IL5) and synoviolin (SYVN1). From a cluster of proteins which demonstrated lower expression in mesenchymal stem cells, we identified serine/arginine rich splicing factor 2 (SRSF2) as an upstream regulator.

2. Materials and methods

2.1. Chemicals and Reagents

LC-MS grade acetonitrile and water were purchased from J.T. Baker (Philipsburg, NJ). Formic acid and RIPA buffer were purchased from Pierce (Rockford, IL). Iodoacetamide (IAA), dithiothreitol (DTT), triethylammonium bicarbonate (TEAB) were obtained from Sigma–Aldrich (St. Louis, MO). Sequencing grade trypsin was purchased from Promega (Madison, WI), and PMSF from CalBiochem (Darmstadt, Germany). All chemicals were used without further purification.

2.2. Cell culture conditions

Isolation of GSCs from patient tumors was performed as previously described [19] in accordance with the institutional review board of The University of Texas M.D. Anderson Cancer Center, and are named in the order they were acquired. GSCs were cultured according to previously published methods [19,35]. Upon dissociation of cells, GSCs were enriched using CD133 via flow cytometry. CD133+ cells are grown in serum-free medium as neurospheres as previously described [21,22]. All cell lines were tested to exclude the presence of *Mycoplasma* infection.

2.3. Proteomic analysis of GSCs

Sample preparation and nanoLC–MS/MS analysis of GSCs was performed as previously described [34]. Briefly, protein (100 μg) isolated from 2×10^6 cells was reduced (TCEP) and alkylated (iodoacetamide). After precipitation using four volumes (440 μL) of ice cold acetone for 2 h at −20 °C, protein was resuspended in 8 M urea (12.5 μL) and digested with trypsin (10 μg in 87.5 μL of TEAB buffer) for 24 h at 37 °C.

Chromatographic separation and mass spectrometric analysis was performed with a nanoLC chromatography system (Easy-nLC 1000, Thermo Scientific), coupled on-line to a hybrid linear iontrap–Orbitrap mass spectrometer (Orbitrap Elite, Thermo Scientific) through a Nano-Flex II nanospray ion source (Thermo Scientific) as previously described [34]. Briefly, samples were analyzed in groups of block-randomized triplicates [36], with three GSCs and M37 (mixed control sample consisting of equal protein from 37 cell lines) in each group. Each block consisted of one technical replicate of each GSC and the M37; the run order for each block was randomized so that data acquisition was not performed in the same order for any of the three blocks. A total of three blocks was acquired for each group of samples, resulting in acquisition of three data files for each GSC and M37. Peptides (1 μg cell protein digest) were separated by gradient elution using a C_{18} column (10 cm × 75 μm ID,15 μm tip, ProteoPep II, 5 μm, 300 Å, New Objective) using a 4 h gradient. Mobile phases were 0.1% formic acid in water (A) and 0.1% formic acid in acetonitrile (ACN; B). All nanoLC–MS/MS data were acquired using XCalibur, version 2.7 SP1 (Thermo Fisher Scientific) using a Top 10 HCD method as previously described [34]. The data files have been deposited into ProteomeXchange repository (PXD001890) [37–40].

2.4. Bioinformatic analysis

Data files were analyzed as previously described [34]. Instrument .raw files for each experimental block were imported into Progenesis LC–MS software (version 18.214.1528, Nonlinear Dynamics) for *m/z* and retention time alignment. This process combines observations for all samples in the block as single measurements for each peptide feature, which allows the best peptide spectrum match for a particular peptide feature to be projected onto all runs within the experimental block. Next, the top 5 spectra for each feature were exported as a combined .mgf file for database searching in PEAKS [41–43] (version 6, Bioinformatics Solutions Inc., Waterloo, ON) and Mascot (version 2.3.02, Matrix Science). Database searches were performed as previously described [34] (10 ppm parent ion tolerance, 0.025 Da fragment ion tolerance, fixed carbamidomethyl cysteine, variable oxidation (methionine), deamidation (asparagine, glutamine) and phosphorylation (serine, threonine, tyrosine), with a maximum of three post-translational modifications per peptide; trypsin with two missed cleavages). Peptide-spectrum matches were then exported from PEAKS as a .xml file and re-imported into Progenesis LC–MS in order to assign peptide-spectrum matches to features. After filtering to remove peptide-spectrum matches below 95% peptide probability (as calculated in PEAKS, using the Peptide Prophet algorithm [44]), manual conflict resolution was performed by removing lower scoring peptide spectrum matches in order to ensure that a single unique peptide sequence was assigned to each feature. Feature intensities were normalized using the default normalization algorithm in Progenesis LC-MS (http://www.nonlinear.com/progenesis/qi-for-proteomics/v2.0/faq/how-normalisation-works.aspx), and normalized peptide intensity data was exported and filtered to remove non-unique peptides, methionine-containing peptides [45], and all modified peptides except those containing cysteine carbamidomethylation. Peptide intensities were imported into DanteR (version 0.1.1) [46,47] for protein quantification as previously described [34]. Briefly, intensities for peptides with the same sequence were combined into a single entry by summation, in order to correct for MS1-level misalignment and to fold together measurements representing multiple charge states of the same peptide. The resulting peptide intensities were $\log_2$-transformed and combined to generate protein abundances (RRollup) without considering proteins with a single peptide assignment. Default settings were used: 50% minimum presence of at least one peptide, minimum dataset presence 3, *p*-value cutoff of 0.05 for Grubbs' Test, minimum of 5 peptides for Grubbs' Test. A one-way ANOVA was performed for each experimental block, relative to M37, to obtain estimated fold changes, and *p*-values were corrected for multiple testing [48]. In order to compare results across experimental blocks, estimated protein fold changes from all experimental blocks were standardized to correct for analytical differences, and the resulting standardized fold changes were imported into Ingenuity Pathway Analysis. Resulting z-scores for upstream regulators and biological and disease functions for all cell lines were exported and collated. After filtering to remove entries with no missing values, unsupervised hierarchical clustering of proteins was performed using a Euclidean distance metric and a Ward linkage metric in Mass Profiler Pro (Agilent, Santa Clara, CA). After filtering to remove entries with <20% missing values, unsupervised hierarchical clustering of upstream regulators was performed using a Euclidean distance metric and an average linkage metric in DanteR.

For additional analysis of biological function, Gene Ontology (GO) analysis was performed using the Database for Annotation, Visualization and Integrated Discovery (DAVID) webtool [32,33]. For each cell line, the proteins were separated into lists of proteins which were increased and decreased relative to mixed control.

Each list was uploaded into the DAVID webtool for separate analysis in order to generate lists of biological functions impacted by changes in protein expression. The Catalog of Somatic Mutations in Cancer (COSMIC) database [27–31] was queried in order to compare our results to known transcript-level variations in sequence and copy-number variation (CNV) associated with GBM tumor samples.

3. Results

3.1. Experimental design

The purpose of our study was to perform a comparison of 35 GSCs at the protein level in order to see if unsupervised hierarchical clustering of protein expression levels was comparable to similar analysis performed on genomic data, and if this clustering was comparable to transcript-based TCGA classification of cell lines. We initially started with 37 cell lines; however, due to low protein yield, two cell lines were removed from the final analysis. Due to the inherent controversy in choosing a normal control for GSCs, we designed a study in which we created a mixed control sample consisting of equal protein from each of the GSC lines. In order to minimize technical difficulties arising from analysis of a large number of cell lines, the 35 GSCs were divided into subgroups consisting of three cell lines plus the mixed control sample (Fig. 1). The GSCs and mixed control were analyzed by nanoLC–MS/MS in block-randomized fashion with triplicates of each cell line analyzed across three separate blocks [36] in order to minimize confounding effects associated with data acquisition, and each subgroup was quantified separately, with fold changes calculated relative to the mixed control sample. Finally, the calculated fold changes were collated and standardized in order to correct for confounding effects relating to instrument drift over time. A total of 2820 proteins were quantified across all GSCs, with 2670 meeting a significance cutoff of $p < 0.05$ in at least one cell line. A complete list of quantified proteins can be found in Supplementary Table 1.

(All supplementary material related to this article can be found, in the online version, at http://dx.doi.org/10.1016/j.euprot.2015.06.008.)

Because the GSCs were enriched for CD133 via flow cytometry and have been previously shown to exhibit stem-like properties, we assessed our data for the presence of CD133 and other stem cell markers. Nestin, an intermediate filament protein, was identified in all cell lines and showed a significant fold change relative to M37 ($p < 0.05$, fold change >2) in only 15/35 cell lines. No specific trend was observed regarding GSC classification and nestin expression. CD133 itself was not found in our quantitative data. This may be due to the fact that it is a membrane protein with five transmembrane domains. In addition, it is a glycoprotein. Because the GSCs were not treated with PNGase F before analysis, we would not expect to identify heavily glycosylated proteins. Sox-2 was also not identified. This is also not surprising, since it is a transcription factor and exhibits low copy numbers within cells.

We recently reported preliminary results for chromosome 19 proteins in a subgroup of the GSCs [34]. Our method was validated by finding that a cell line analyzed twice, in an early subgroup and again in a later subgroup, clustered together in both principal components analysis (PCA) and unsupervised hierarchical clustering (Supplementary Fig. 1). This report expands these findings to include proteins in all cell lines from all chromosomes. Previously reported findings are included again in order to provide a complete and more detailed comparison of the GSCs.

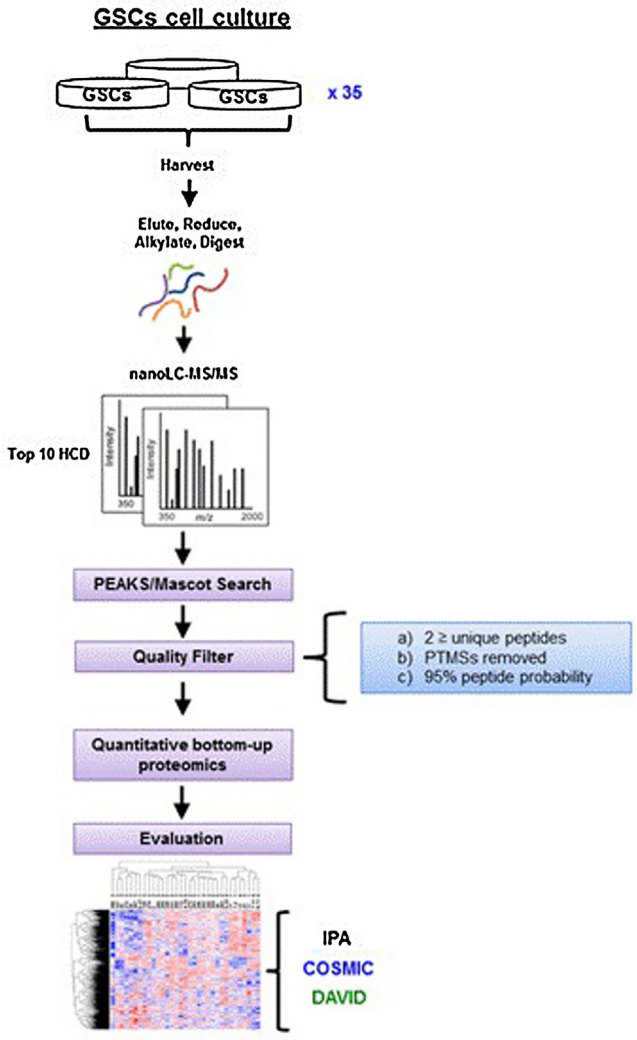

Fig. 1. Workflow for proteomics analysis of GSCs. Patient-derived GSCs were lysed and processed for nanoLC–MS/MS analysis as described in Section 2, Materials and methods. GSCs were analyzed in 13 groups, with each group containing 3 GSCs and a control sample (M37). Within each group, samples were analyzed in triplicate, employing block randomization in order to eliminate potential sources of bias in data acquisition. The resulting .raw files were aligned by accurate mass and time for label-free quantitative proteomics, and protein-level fold changes relative to M37 were calculated by one-way ANOVA (DanteR). The resulting protein fold changes relative to M37 were used for bioinformatic characterization of GSCs.

3.2. Analysis of Biological Function

GO and IPA analyses were performed on significantly changed proteins ($p < 0.05$) in each cell line. For GO analysis, protein lists were separated based upon decreased or increased fold change relative to mixed control and analyzed separately using the DAVID webtool [32,33]. A complete list of the top biological functions from GO can be found in Supplementary Table 2. The number of proteins with GO terms related to RNA processing was among the most significantly enriched (128 proteins with higher expression in GSC8-11, 155 proteins with lower expression for GSC126 compared to M37). When ranked by number of cell lines impacted, the GO term represented across the greatest number of cell lines was generation of precursor metabolites and energy (33 cell lines), followed closely by oxidation reduction (32 cell lines), glycolysis (32 cell lines) and cellular carbohydrate catabolic processes (32 cell lines).

The table of identified proteins and their relative expression values for each cell line was uploaded into IPA for further elucidation of biological function through a Core Analysis. HumanCyc metabolic pathways [49] are used in IPA, making IPA

findings complementary to KEGG findings from DAVID. Canonical pathways which were found to be significant ($p < 0.05$) in the highest number of cell lines included protein ubiquitination pathway (33 cell lines), gluconeogenesis I (33 cell lines), glycolysis I (33 cell lines), regulation of cellular mechanics by calpain protease (33 cell lines), signaling by Rho family GTPases (33 cell lines), caveolar-mediated endocytosis signaling (32 cell lines), mitochondrial dysfunction (32 cell lines), and epithelial adherens junction signaling (32 cell lines). A complete list of enriched canonical pathways can be found in Supplementary Table 3.

Similarly, a comparison was made for significant enrichment of diseases and biological functions ($p < 0.05$) in IPA. Those which were found to be significant in the largest number of cell lines included folding of protein (35 cell lines), apoptosis (34 cell lines), apoptosis of tumor cell lines (34 cell lines), cell death (34), cell death of tumor cell lines (34 cell lines), cell viability (34 cell lines), metabolism of protein (34 cell lines), necrosis (34 cell lines), and proliferation of tumor cell lines (34 cell lines). A complete list of affected biological functions can be found in Supplementary Table 4.

In addition to *p*-values, IPA also provides z-scores for diseases and biological functions. These z-scores provide a measure of predicted activation or inhibition based upon observed protein fold changes; those with z-scores < -1.50 were predicted to show significant inhibition, while z-scores >1.50 were predicted to be significantly activated. Experimentally observed gene expression or transcription events, associated with literature-derived regulation (activating or inhibiting) serve as the basis for inference. Likewise, literature-derived gene-level effects on diseases and biological functions are used to provide an indication of activation or inhibition. Given the observed differential regulation of a gene (up or down) in a dataset, the activation state for a downstream gene or biological process is determined based upon information contained in the Ingenuity Knowledgebase. Diseases and biological functions with significant z-scores in the highest number of cells included viral infection (16 cell lines), migration of cells (16 cell lines), organismal death (16 cell lines), modification of reactive oxygen species (15 cell lines), cell movement of tumor cell lines (15 cell lines), and migration of tumor cell lines (14 cell lines). Upstream regulators predicted to be significantly inhibited or activated included INSR (27 cell lines), MYC (23 cell lines), retinoblastoma-associated protein (RB1, 22 cell lines), TP53 (21 cell lines), HNF4A (19 cell lines), MYCN (19 cell lines), IL5 (17 cell lines), and SYVN1 (14 cell lines). A complete list of activated and inhibited biological diseases and functions can be found in Supplementary Table 5.

Upstream analysis, also performed in IPA, provided a list of inferred upstream regulators based upon measured fold changes for each cell line. The goal of the IPA Upstream Regulator analytic is to identify a putative cascade of upstream transcriptional regulators (TRs) that can explain the observed gene expression changes in a user's dataset, which can help illuminate the biological activities occurring in the tissues or cells being studied. IPA's definition of upstream TR is quite broad and includes any molecule that can affect the expression of other molecules. This means that IPA-defined upstream regulators can be almost any type of molecule, from transcription factor, to microRNA, kinase, compound, or drug.

For each potential TR, two statistical measures, an overlap *p*-value and an activation z-score are computed. The overlap *p*-value assigns likely upstream regulators based on significant overlap between dataset genes and known targets regulated by a TR. The purpose of the overlap *p*-value is to identify upstream regulators that are able to explain observed gene expression

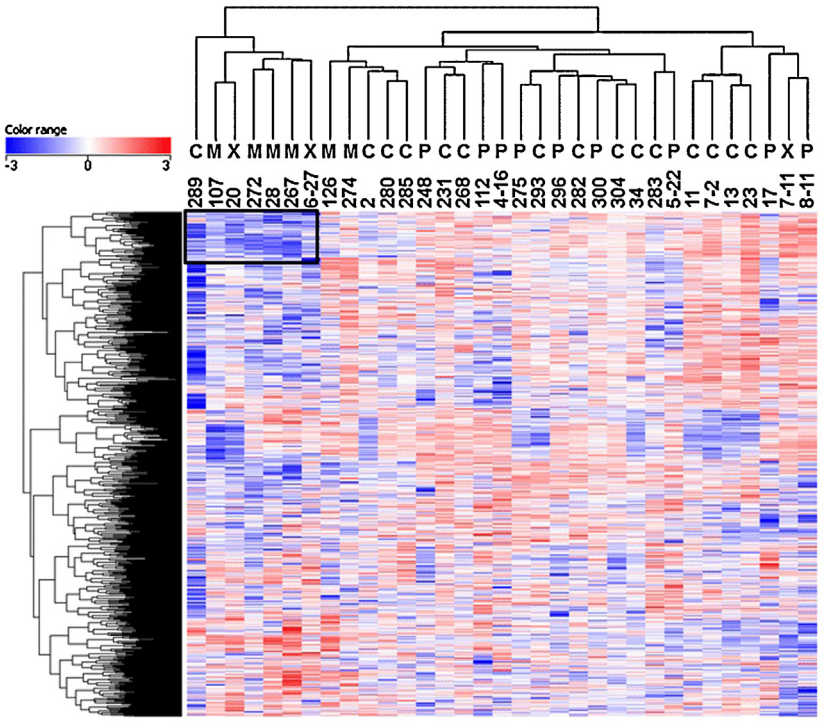

Fig. 2. Unsupervised hierarchical clustering of protein-level fold changes for GSCs. Protein fold changes were standardized to account for analytical variation, and unsupervised hierarchical clustering was performed for those proteins present in >80% of the cell lines. Two cell lines were removed from this analysis due to a low number of significant proteins. TCGA classification of cell lines [C (classical), M (mesenchymal), P (proneural), and X (unclassified)], as determined at MDACC, was added to the heat map in order to compare to results based on transcript-level classification. Red indicates protein levels higher than in M37, while blue represents protein levels lower than in M37. The protein cluster encompassed by the black box represents a proteomic signature of proteins decreased in a cluster of cell lines enriched for mesenchymal GSCs. (For interpretation of the references to color in this figure legend, the reader is referred to the web version of this article.)

changes, but no activation or inhibition is predicted. Upstream regulators which were found to be significant (overlap p-value <0.05) in the largest number of cell lines included cellular tumor antigen p53 (TP53), myc proto-oncogene protein (MYC), huntingtin (HTT), hepatocyte nuclear factor 4-alpha (HNF4A), amyloid beta A4 protein (APP), N-myc proto-oncogene protein (MYCN), insulin receptor (INSR), E3 ubiquitin-protein ligase synoviolin (SYVN1), interleukin-3 (IL3), fragile X mental retardation protein 1 (FMR1), adenosine receptor A2a (ADORA2A), aryl hydrocarbon receptor nuclear translocator (ARNT), Cu-Zn superoxide dismutase (SOD1), and interleukin-5 (IL5). A complete list of significant predicted upstream regulators can be found in Supplementary Table 6.

The activation z-score is used to infer likely activation states of upstream regulators based on comparison with a model that assigns random regulation directions. Under ideal circumstances, the activation z-score can also be used to predict upstream regulators independently from the overlap p-value, based on significant pattern match of up/down regulation. A complete list of upstream regulators can be found in Supplementary Table 7.

3.3. Classification of GSCs by unsupervised hierarchical clustering

In order to determine common patterns of molecular-level behavior amongst the GSCs based upon proteomics analysis, unsupervised hierarchical clustering was performed for proteins (by $\log_2$ fold change, Fig. 2) and for upstream regulators (by z-score, Fig. 3). Next, each cell line was labeled with its TCGA classification, as assigned by our collaborators at MDACC [50], in order to see if a characteristic signature was present for one or more classes of cells. In both instances, enrichment was seen for mesenchymal cell lines. In the protein heat map (Fig. 2), two classical (GSCs 289 and 6-27) and five mesenchymal cell lines (GSCs 107, 20, 272, 28, and 267) were grouped together (*left, box*). In the heat map for predicted upstream regulators (Fig. 3), two classical cell lines (GSCs 231 and 285), four mesenchymal cell lines (GSCs 107, 267, 28, and 20) and one unclassified cell line (GSC 126) were grouped together (*right*).

3.4. Analysis of a protein cluster down-regulated in mesenchymal GSCs

Because the top protein cluster (outlined in black, Fig. 2) stood out as being characteristically decreased in mesenchymal cell lines, the list of 74 proteins (Supplementary Table 8) in this cluster was extracted for further analysis. GO analysis as performed using the DAVID webtool (Fig. 4) revealed that a majority of these proteins were involved in RNA splicing. In IPA, significant ($p < 0.05$) canonical pathways included granzyme B signaling, DNA double-strand break repair by non-homologous end joining, estrogen receptor signaling, and DNA methylation and transcriptional repression signaling. Top molecular and cellular functions included RNA post-transcriptional modification (32 proteins), cellular growth and proliferation (44 proteins), protein synthesis (16 proteins), gene expression (35 molecules), and cell morphology (10 proteins). The top four upstream regulators (p-value of overlap <0.05) were the transcription regulators serine/arginine rich splicing factor 2 (SRSF2), E2F1, MYC, and E2F4.

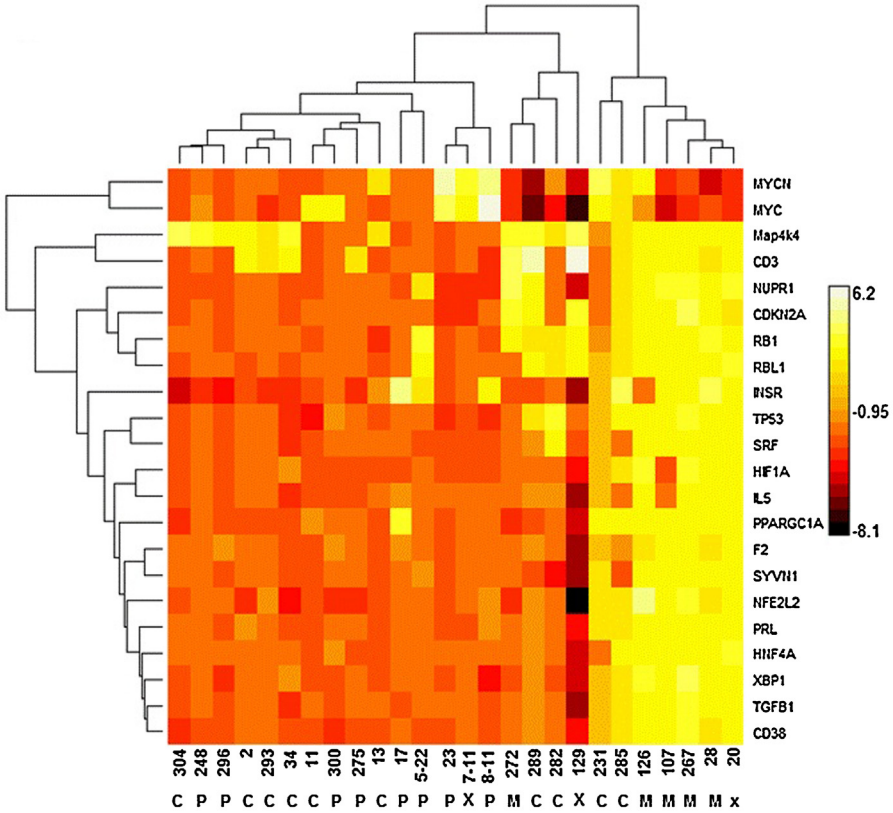

Fig. 3. Unsupervised hierarchical clustering of putative upstream regulators for GSCs**.** Unsupervised hierarchical clustering of putative upstream regulators by z-score as calculated by Ingenuity Pathway Analysis. Before clustering, the list was filtered to remove upstream regulators present in <80% of the cell lines, and cell lines were removed which did not contain 80% of the listed upstream regulators. TCGA classification of cell lines [C (classical), M (mesenchymal), P (proneural), and X (unclassified)], as determined at MDACC, was added to the heat map. White/yellow indicates higher z-scores, while red/black represents lower z-scores. (For interpretation of the references to color in this figure legend, the reader is referred to the web version of this article.)

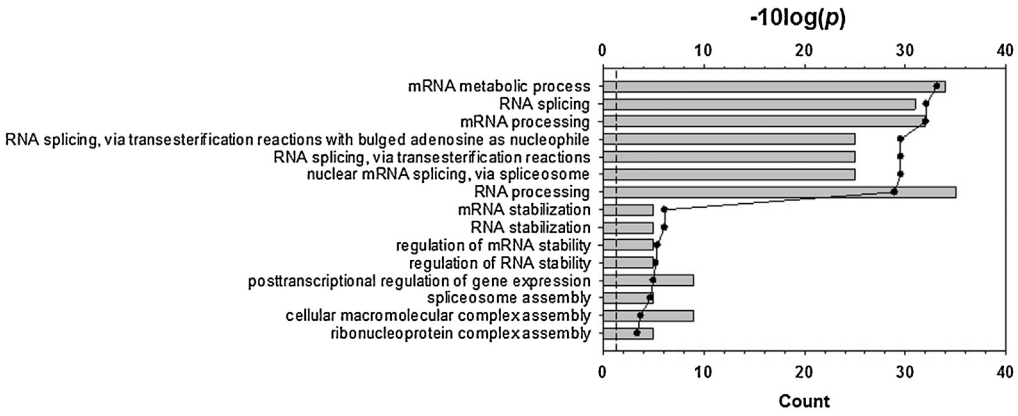

Fig. 4. GO Biological Processes analysis of protein cluster decreased in mesenchymal GSCs. Bar chart represents classification of GO biological processes as determined by DAVID. Bars represent the number of proteins in the specified category, while the black line indicates statistical significance ($-10\log(p)$).

4. Discussion

Herein we report the results of a study in which we performed label-free quantification of 37 GSCs. Due to the inherent challenges of comparison when there is no clear normal control sample, quantification was performed relative to a mixed control sample (M37) containing equal protein from each of the cell lines studied. Ultimately, due to problems with low protein levels in two of the original samples, 35 samples were quantified. Cell lines were analyzed in groups of 3 plus M37 in block-randomized analytical triplicates. Fold changes relative to M37 were used to compare and characterize the GSCs. Because the GSCs are quantified relative to an average protein signature for all cell lines, proteins with common expression changes across all cell lines will not be measured as significant. However, proteins which are different from the average would be expected to provide a characteristic proteomic signature for each cell line. Shared proteomic signatures should also be discernible for similar GSCs, facilitating the identification of potential therapeutic targets.

Our results represent the first reported relative protein quantification for 35 GSC lines. Our analysis identified significant changes in a number of proteins known to be dysregulated in glioma. These include two proteins whose overexpression has been linked to temozolomide (TMZ) resistance in GBM: galectin-1 (LGALS1) [51] and EGFR [52,53]. In addition, our results for affected biochemical pathways are consistent with those which have been previously reported. For instance, glycolysis and gluconeogenesis have been shown to be upregulated in mesenchymal GSCs [54]. Confirmation of known findings gives greater confidence in the novel findings in our dataset, which may be used as a basis for further mechanistic studies into GBM chemoresistance.

Several of the GSCs from this study have been previously characterized at the transcript level [50]. Since protein and transcript levels do not tend to correlate closely [55–58], we would not expect the cells to cluster in the same manner at the protein and transcript levels. The transcripts [50] and proteins are similar in that two clusters were observed in unsupervised hierarchical clustering, but a slight difference was seen in terms of the cell lines that were clustered together. In both instances, GSCs 6-27, 20 and 28 were clustered together. Of the other common cell lines between the two studies, GSCs 2 and 17 were in cluster 1 in the transcriptomic data [50] and cluster 2 in the proteomic data. Multiple cell lines exhibit mixed transcript-level TCGA profiles [50], so it is not surprising to see similar behavior at the protein level. For example, GSC6-27 was reported to display characteristics of both mesenchymal and proneural subtypes at the transcript level [50], which helps to explain its appearance in a cluster of mesenchymal cell lines.

4.1. Potential role of SYMPK in glioma

Our preliminary results demonstrated the first report of SYMPK as a potential protein-level biomarker for glioma in GSCs 2, 11 and 13 [34], although it has been previously implicated in lung cancer [59] and colorectal cancer [60]. Herein we report that, in addition to the previously published results, we have measured significant fold changes in GSCs 231 and 296. In the GSCs, significant fold changes relative to M37 were measured for five cell lines, four of which are classical (GSCs 2, 11, 13 and 231) and one of which is proneural (296). SYMPK was found to be significantly increased relative to M37 in three of the classical cell lines (GSCs 2, 11 and 13) and in the proneural cell line GSC296, while it was decreased in the remaining cell line (GSC231). In COSMIC, for 166 patient tumor samples, both overexpression (five samples) and underexpression (three samples) of SYMPK was seen. Therefore, further study is warranted in order to determine the role of SYMPK in GBM. Initial studies should focus on orthogonal validation using techniques such as peptide MRM or western blotting. Orthogonal validation is especially important due to the nature of the quantitative comparison. In addition to confirming significant changes in SYMPK in GSCs 2, 11, 13, 231 and 296, orthogonal validation might reveal significant changes in protein expression in other cell lines.

SYMPK has been found in both the nucleus and in tight junction complexes (TJ) [61]. As a nuclear protein, it is involved in histone 3′ mRNA maturation as a part of the polyadenylation machinery [62]. As a TJ protein, it has been found to modulate cellular architecture and has been shown to play a role in maintaining mitotic fidelity through the support of spindle formation [59]. In human colorectal cancer cells, increased expression of SYMPK in the nucleus was shown to promote tumorigenesis through upregulation of claudin-2 [60]. A pangenomic loss-of-function screening assay identified SYMPK as a potent chemosensitizer; reduced levels of SYMPK caused non-small-cell lung carcinoma cells to be sensitive to lower doses of paclitaxel [63]. In a follow-up study, knockout of SYMPK was shown to inhibit tumor growth through induction of mitotic defects, both in vitro and in vivo, while not affecting normal cells [60]. Given these results, SYMPK might prove to be a useful target in the design of a novel chemotherapy-based treatment strategy for GBM. The commonly accepted treatment protocol for GBM involves surgical resection, followed by chemotherapy treatment (usually with TMZ as adjuvant chemotherapy), and radiation [6], but a recent study has demonstrated the effectiveness of combination therapies using TMZ and paclitaxel [64]. Another

study, using paclitaxel poliglumex in combination with TMZ and concurrent radiation, showed some promise in terms of overall survival, but the drugs could not be combined safely due to toxicity issues [65]. Therefore, it would be useful to measure the effectiveness of SYMPK knockdown to enhance the effectiveness of a combined chemotherapeutic regimen in GSCs.

4.2. Newly reported upstream regulators SYVN1 and IL5

Upstream analysis, as performed in IPA, identifies upstream regulators whose activation or inhibition is consistent with measured protein fold changes. In our study, several species known to be dysregulated in glioma were identified as upstream regulators in both tumors and glioma cell lines, including MYC [66–71], MYCN [72,73], TP53 [74–77], and RB1 [71]. Identification of these known upstream regulators provides greater confidence in the novel upstream regulators identified in our study, SYVN1 and IL5. It is important to emphasize that upstream analysis provides an indication of protein activity rather than expression level, although changes in expression may accompany activation or inhibition. In addition, our z-scores were calculated from fold changes relative to M37. Although the results indicate a similar pattern of behavior for several mesenchymal cell lines, the novel findings in this study would require activity and/or functional assays for validation.

SYVN1 is an E3 ubiquitin ligase, transferring ubiquitin specifically from ubiquitin-conjugating enzyme E2 G1 (UBC7) to its substrates, thus promoting their proteasomal degradation. It is involved in ER-associated degradation system, targeting misfolded proteins for degradation. Within the brain, SYVN1 protects neurons from apoptosis by promoting degradation of polyglutamate-expanded huntingtin protein (HTT) and unfolded prosaposin receptor GPR37 (GPR37). Perhaps most significantly, SYVN1 acts as a negative regulator of TP53 by sequestering it in the cytoplasm and promoting its degradation. Through degradation of TP53, SYVN1 plays a critical role in regulating transcription, cell cycle regulation and apoptosis [78].

The association between TP53 and SYVN1 makes the prediction of SYVN1 as an upstream regulator particularly intriguing. According to the COSMIC database, 25% of Astrocytoma Grade IV (GBM) samples were found to have mutations in TP53. This number is lower than the 87% mutation frequency cited by TCGA [13]. In terms of expression data, nine out of 166 samples (~5.5%) demonstrated overexpression of TP53, while five samples (3%) showed overexpression. It has been found that mutations in TP53 lead to decreased degradation of p53 protein oligomers, resulting in increased accumulation in the nucleus [75]. Therefore, the role of SYVN1 in GBM merits further study.

IL5 is intriguing due to reports linking levels of this cytokine with LGALS1, a protein that has been long known to suppress immune response through apoptosis of T cells [79]. Previous studies in GBM have demonstrated that increased levels of LGALS1 at the tumor margin are linked to invasivity [80], a process that is believed to occur through suppression of the innate immune response [81]. Moreover, LGALS1 and IL5 have been linked in other types of cancer. A recent study of pancreatic stellate cell lines, the origin of elevated LGALS1 found in pancreatic ductal adenocarcinoma stromal tissue, showed a correlation between elevated LGALS1 expression and increased levels of IL5 [82]. Further, both knockdown and inhibition of LGALS1 reversed the elevation in IL5 levels. Given these findings, we believe that further study, aimed at determining a possible role of IL5 in invasivity of GBM, is warranted.

4.3. SRSF2 linked to chemoresistance

In our analysis, a distinctive proteomic signature was present for a cluster of proteins that were decreased in several of the mesenchymal cell lines. Processes relating to RNA splicing were highly represented in this cluster, and SRSF2 was implicated as an upstream regulator. SRSF2 itself was a part of this cluster and demonstrated lower relative protein expression. In the COSMIC database, for a total of 712 Grade IV astrocytoma (GBM) tumor samples, no RNA-level copy number variation, overexpression, or underexpression were reported for SRSF2. This discordance is not surprising; it is well known that correlation between protein and transcript data is not high. Regulation of protein abundance is not controlled solely by RNA transcription; factors such as protein and transcript stability both come into play. Studies conducted across a variety of species have shown poor to moderate correlation between protein and transcript [55–58]. Therefore, our findings serve to further highlight the utility of quantitative proteomics in the quest for therapeutic targets. As is the case with other reported findings, orthogonal validation is an important and necessary step in this process. Western blotting and/or peptide MRM work would be a critical step in confirming the measured decrease in SRSF2 in mesenchymal cell lines and might also uncover significant changes in expression in other cell lines.

SRSF2 is involved in pre-mRNA splicing and is a required member of the ATP-dependent splicing complex. Although there are no literature reports of SRSF2 associated with GBM, SRSF2 has been associated with other cancers. Recent reports have linked SRSF2 to chemoresistance in hepatocellular carcinoma [83] and bladder cancer [84,85]. The basis of SRSF2 chemoresistance is related to upregulation of miR-193a-3p, which has been found in a recent study to be upregulated in hypoxia and in GBM tumor samples [86]. Upregulation of miR-193a-3p was shown to lead to suppression of SRSF2 [84]. Given the relatively lower expression of SRSF2 in our mesenchymal GSCs, miR-193a-3p is worthy of further study.

Cellular levels of SRSF2 are regulated by an acetylation/phosphorylation signaling network [87]. Proteasomal degradation of SRSF2 is controlled by acetylation on lysine 52, catalyzed by histone acetyltransferase KAT5 [87]. This effect is counterbalanced by the deacetylase HDAC6. Moreover, KAT5 was found to negatively control SRSF2 phosphorylation [87]. Because SRSF2 is known to inactivate TP53, this crosstalk of post-translational modifications is critical in carcinogenesis. Phosphorylation of SRSF2 by SRSF protein kinase 2 (SRPK2) inactivates TP53, resulting in cyclin D1 expression and neuronal apoptosis [88]. Therefore, in addition to a measurement of protein expression, it would be critical to study SRSF2 phosphorylation and acetylation in the GSCs.

5. Conclusions

We have demonstrated the utility of using a mixed control sample in the relative quantification of GSCs. Through our analysis, we have identified GSC proteins with known association to GBM, as well as several novel ones, including SYMPK, SYVN1, and IL5. These proteins all connect, both directly and indirectly, to TP53 (Fig. 5). This combination of known and novel proteins demonstrates the hypothesis-generating power of our approach. Further studies are warranted to evaluate our novel findings in GSCs.

6. Conflict of interest

The authors do not have any conflicts of interest to disclose.

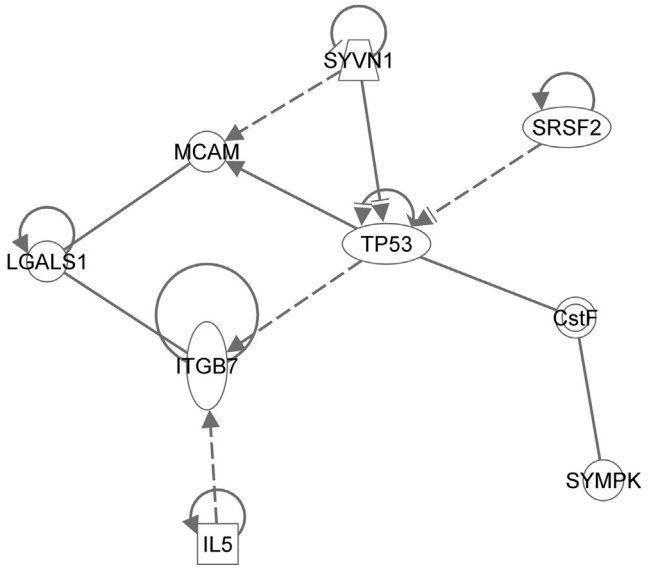

Fig. 5. Network demonstrating connection between novel and known regulators or GBM. A network demonstrating connection of our newly reported proteins SYMPK, SYVN1, IL5, and SRSF2 to known GBM-related proteins TP53 and LGALS1. Solid lines indicate direct interactions, while dashed lines indicate indirect interactions.

7. Author contributions

Conceived and designed experiments: CFL, HL, EM, CLN. Contributed GSCs: EPS. Performed sample preparation and data acquisition: HL, ASS. Performed data analysis: CFL. Wrote the manuscript: CFL, NCW. All authors contributed to and gave approval to the final version of the manuscript.

Acknowledgments

Support from the Cancer Prevention and Research Institute of Texas (CLN) and the University of Texas Medical Branch (CLN) is gratefully acknowledged, as are the Biomolecular Resource Facility Mass Spectrometry Lab (CFL) and the Department of Pharmacology & Toxicology (CFL). EPS was supported by the National Institutes of Health/National Cancer Institute (SPORE Grant No. P50CA127001, R01CA190121). The DanTE software was written by Tom Taverner (t.taverner@gmail.com) and Ashoka Polpitiya for the U.S. Department of Energy (PNNL, Richland, WA, USA, http://omics.pnl.gov/software). Mark R. Emmett, Frederick F. Lang, and Charles A. Conrad are gratefully acknowledged for helpful discussions (CFL).

References

[1] P. Kleihues, W.K. Cavenee, International Agency for Research on Cancer, Pathology and genetics of tumours of the nervous system, World Health Organization Classification of Tumours, Lyon: IARC Press, 2000314.
[2] D.N. Louis, et al., The 2007 WHO classification of tumours of the central nervous system, Acta Neuropathol. 114 (2) (2007) 97–109.
[3] M.E. Berens, A. Giese, " . . . *those left behind.* " Biology and oncology of invasive glioma cells, Neoplasia 1 (3) (1999) 208–219.
[4] A. Giese, et al., Cost of migration: invasion of malignant gliomas and implications for treatment, J. Clin. Oncol. 21 (8) (2003) 1624–1636.
[5] H.J. Scherer, A critical review: the pathology of cerebral gliomas, J. Neurol. Psychiatry 3 (2) (1940) 147–177.
[6] R. Stupp, et al., Radiotherapy plus concomitant and adjuvant temozolomide for glioblastoma, N. Engl. J. Med. 352 (10) (2005) 987–996.
[7] S. Bao, et al., Glioma stem cells promote radioresistance by preferential activation of the DNA damage response, Nature 444 (7120) (2006) 756–760.
[8] S. Facchino, et al., BMI1 confers radioresistance to normal and cancerous neural stem cells through recruitment of the DNA damage response machinery, J. Neurosci. 30 (30) (2010) 10096–10111.
[9] C.G. Hadjipanayis, E.G. Van Meir, Tumor initiating cells in malignant gliomas: biology and implications for therapy, J. Mol. Med. (Berl.) 87 (4) (2009) 363–374.
[10] M.K. Kang, S.K. Kang, Tumorigenesis of chemotherapeutic drug-resistant cancer stem-like cells in brain glioma, Stem Cells Dev. 16 (5) (2007) 837 47.
[11] G. Liu, et al., Analysis of gene expression and chemoresistance of CD133+ cancer stem cells in glioblastoma, Mol. Cancer 5 (2006) 67.
[12] C.W. Brennan, et al., The somatic genomic landscape of glioblastoma, Cell 155 (2) (2013) 462–477.
[13] Cancer Genome Atlas Research Network, Comprehensive genomic characterization defines human glioblastoma genes and core pathways, Nature 455 (7216) (2008) 1061–1068.
[14] J.T. Huse, H.S. Phillips, C.W. Brennan, Molecular subclassification of diffuse gliomas: seeing order in the chaos, Glia 59 (8) (2011) 1190–1199.
[15] H.S. Phillips, et al., Molecular subclasses of high-grade glioma predict prognosis, delineate a pattern of disease progression, and resemble stages in neurogenesis, Cancer Cell 9 (3) (2006) 157–173.
[16] R.G. Verhaak, et al., Integrated genomic analysis identifies clinically relevant subtypes of glioblastoma characterized by abnormalities in PDGFRA, IDH1, EGFR, and NF1, Cancer Cell 17 (1) (2010) 98–110.
[17] B.J. Gill, et al., MRI-localized biopsies reveal subtype-specific differences in molecular and cellular composition at the margins of glioblastoma, Proc. Natl. Acad. Sci. U. S. A. 111 (34) (2014) 12550–12555.
[18] E. Butti, et al., Neurogenic and non-neurogenic functions of endogenous neural stem cells, Front. Neurosci. 8 (2014) 92.
[19] R. Galli, et al., Isolation and characterization of tumorigenic, stem-like neural precursors from human glioblastoma, Cancer Res 64 (19) (2004) 7011–7021.
[20] H.D. Hemmati, et al., Cancerous stem cells can arise from pediatric brain tumors, Proc. Natl. Acad. Sci. U. S. A. 100 (25) (2003) 15178–15183.
[21] S.K. Singh, et al., Identification of a cancer stem cell in human brain tumors, Cancer Res. 63 (18) (2003) 5821–5828.
[22] S.K. Singh, et al., Identification of human brain tumour initiating cells, Nature 432 (7015) (2004) 396–401.
[23] H. Zhu, et al., Oncogenic EGFR signaling cooperates with loss of tumor suppressor gene functions in gliomagenesis, Proc. Natl. Acad. Sci. U. S. A. 106 (8) (2009) 2712–2716.
[24] N. Lindberg, et al., Oligodendrocyte progenitor cells can act as cell of origin for experimental glioma, Oncogene 28 (23) (2009) 2266–2275.
[25] D. Friedmann-Morvinski, et al., Dedifferentiation of neurons and astrocytes by oncogenes can induce gliomas in mice, Science 338 (6110) (2012) 1080–1084.
[26] C. Dufour, et al., Astrocytes reverted to a neural progenitor-like state with transforming growth factor alpha are sensitized to cancerous transformation, Stem Cells 27 (10) (2009) 2373–2382.
[27] S. Bamford, et al., The COSMIC (Catalogue of Somatic Mutations in Cancer) database and website, Br. J. Cancer 91 (2) (2004) 355–358.
[28] S.A. Forbes, et al., COSMIC: exploring the world's knowledge of somatic mutations in human cancer, Nucleic Acids Res. 43 (2015) D805–D811 (Database issue).
[29] S.A. Forbes, et al., The Catalogue of Somatic Mutations in Cancer (COSMIC), Am. J. Clin. Oncol. (2008) April Chapter 10: p. Unit 10.11.
[30] S.A. Forbes, et al., COSMIC: mining complete cancer genomes in the Catalogue of Somatic Mutations in Cancer, Nucleic Acids Res. 39 (2011) D945–D950 (Database issue).
[31] S.A. Forbes, et al., COSMIC (the Catalogue of Somatic Mutations in Cancer): a resource to investigate acquired mutations in human cancer, Nucleic Acids Res. 38 (2010) D652–D657 (Database issue).
[32] D.W. Huang, R.A. Lempicki B.T. Sherman, Systematic and integrative analysis of large gene lists using DAVID bioinformatics resources, Nat. Protoc. 4 (1) (2009) 44–57.
[33] D.W. Huang, et al., DAVID Bioinformatics Resources: expanded annotation database and novel algorithms to better extract biology from large gene lists, Nucleic Acids Res. 35 (2007) W169–W175 (Web Server issue).
[34] C.F. Lichti, et al., Integrated chromosome 1transcriptomic and proteomic data sets derived from glioma cancer stem-cell lines, J. Proteome Res. 13 (1) (2014) 191–199.
[35] H. Jiang, et al., Examination of the therapeutic potential of Delta-2RGD in brain tumor stem cells: role of autophagic cell death, J. Natl. Cancer Inst. 99 (18) (2007) 1410–1414.
[36] A.L. Oberg, O. Vitek, Statistical design of quantitative mass spectrometry-based proteomic experiments, J. Proteome Res. 8 (5) (2009) 2144–2156.
[37] R.G. Cote, et al., The PRoteomics IDEntification (PRIDE) Converter 2 framework: an improved suite of tools to facilitate data submission to the PRIDE database and the ProteomeXchange consortium, Mol. Cell. Proteomics 11 (12) (2012) 1682–1689.
[38] H. Hermjakob, R. Apweiler, The Proteomics Identifications Database (PRIDE) and the ProteomExchange Consortium: making proteomics data accessible, Expert Rev. Proteomics 3 (1) (2006) 1–3.
[39] T. Ternent, et al., How to submit MS proteomics data to ProteomeXchange via the PRIDE database, Proteomics 14 (20) (2014) 2233–2241.
[40] J.A. Vizcaino, et al., ProteomeXchange provides globally coordinated proteomics data submission and dissemination, Nat. Biotechnol. 32 (3) (2014) 223–226.
[41] Y. Han, B. Ma, K. Zhang, SPIDER: software for protein identification from sequence tags with de novo sequencing error, J. Bioinform. Comput. Biol. 3 (3) (2005) 697–716.
[42] B. Ma, et al., PEAKS: powerful software for peptide de novo sequencing by tandem mass spectrometry, Rapid Commun. Mass Spectrom. 17 (20) (2003) 2337–2342.

[43] J. Zhang, et al., PEAKS DB: de novo sequencing assisted database search for sensitive and accurate peptide identification, Mol. Cell. Proteomics 111 (4) (2012) M111.010587.
[44] R.A. Keller, et al., Analytical applications of single-molecule detection, Anal. Chem. 74 (11) (2002) 316A–324A.
[45] R.J. Perrin, et al., Quantitative label-free proteomics for discovery of biomarkers in cerebrospinal fluid: assessment of technical and inter-individual variation, PLoS One 8 (5) (2013) e64314.
[46] Y. Karpievitch, et al., A statistical framework for protein quantitation in bottom-up MS-based proteomics, Bioinformatics 25 (16) (2009) 2028–2034.
[47] A.D. Polpitiya, et al., DAnTE: a statistical tool for quantitative analysis of -omics data, Bioinformatics 24 (13) (2008) 1556–1558.
[48] Y. Benjamini, Y. Hochberg, Controlling the False Discovery Rate: A Practical and Powerful Approach to Multiple Testing, J. R. Statist Soc. Ser. B (Methodol.) 57 (1) (1995) 289–300.
[49] P. Romero, et al., Computational prediction of human metabolic pathways from the complete human genome, Genome Biol. 6 (1) (2005) R2.
[50] K.P. Bhat, et al., Mesenchymal differentiation mediated by NF-kappaB promotes radiation resistance in glioblastoma, Cancer Cell 24 (3) (2013) 331–346.
[51] M. Le Mercier, et al., Evidence of galectin-1 involvement in glioma chemoresistance, Toxicol. Appl. Pharmacol. 229 (2) (2008) 172–183.
[52] P. Leuraud, et al., Distinct responses of xenografted gliomas to different alkylating agents are related to histology and genetic alterations, Cancer Res. 64 (13) (2004) 4648–4653.
[53] P.H. Huang, et al., Quantitative analysis of EGFRvIII cellular signaling networks reveals a combinatorial therapeutic strategy for glioblastoma, Proc. Natl. Acad. Sci. U. S. A. 104 (31) (2007) 12867–12872.
[54] S. Zheng, et al., A survey of intragenic breakpoints in glioblastoma identifies a distinct subset associated with poor survival, Genes Dev. 27 (13) (2013) 1462–1472.
[55] A. Alli Shaik, et al., Functional mapping of the zebrafish early embryo proteome and transcriptome, J. Proteome Res. 13 (12) (2014) 5536–5550.
[56] J. Gunaratne, et al., Extensive mass spectrometry-based analysis of the fission yeast proteome: the Schizosaccharomyces pombe PeptideAtlas, Mol. Cell. Proteomics 12 (6) (2013) 1741–1751.
[57] N. Nagaraj, et al., Deep proteome and transcriptome mapping of a human cancer cell line, Mol. Syst. Biol. 7 (2011) 548.
[58] S.P. Schrimpf, et al., Comparative functional analysis of the Caenorhabditis elegans and Drosophila melanogaster proteomes, PLoS Biol. 7 (3) (2009) e48.
[59] K.M. Cappell, et al., Symplekin specifies mitotic fidelity by supporting microtubule dynamics, Mol. Cell Biol. 30 (21) (2010) 5135–5144.
[60] M. Buchert, et al., Symplekin promotes tumorigenicity by up-regulating claudin-2 expression, Proc. Natl. Acad. Sci. U. S. A. 107 (6) (2010) 2628–2633.
[61] B.H. Keon, et al., Symplekin, a novel type of tight junction plaque protein, J. Cell Biol. 134 (4) (1996) 1003–1018.
[62] N.G. Kolev, J.A. Steitz, Symplekin and multiple other polyadenylation factors participate in 3'-end maturation of histone mRNAs, Genes Dev. 19 (21) (2005) 2583–2592.
[63] A.W. Whitehurst, et al., Synthetic lethal screen identification of chemosensitizer loci in cancer cells, Nature 446 (7137) (2007) 815–819.
[64] S. Ni, et al., Biodegradable implants efficiently deliver combination of paclitaxel and temozolomide to glioma C6 cancer cells in vitro, Ann. Biomed. Eng. 42 (1) (2014) 214–221.
[65] S. Jeyapalan, et al., Paclitaxel poliglumex, temozolomide, and radiation for newly diagnosed high-grade glioma: A Brown University Oncology Group Study, Am. J. Clin. Oncol. 37 (5) (2014) 444–449.
[66] J. Trent, et al., Evidence for rearrangement, amplification, and expression of c-myc in a human glioblastoma, Proc. Natl. Acad. Sci. U S A 83 (2) (1986) 470–473.
[67] N. Blin, et al., Enhanced expression of four cellular oncogenes in a human glioblastoma cell line, Cancer Genet. Cytogenet. 25 (2) (1987) 285–292.
[68] H.H. Engelhard 3rd, A.B. t. Butler, K.D. Bauer, Quantification of the c-myc oncoprotein in human glioblastoma cells and tumor tissue, J. Neurosurg. 71 (2) (1989) 224–232.
[69] S. Patt, et al., Chromosomal changes and correspondingly altered proto-oncogene expression in human gliomas. Value of combined cytogenetic and molecular genetic analysis, Anticancer Res. 13 (1) (1993) 113–118.
[70] H. Shindo, et al., Stabilization of c-myc protein in human glioma cells, Acta Neuropathol. 86 (4) (1993) 345–352.
[71] H.E. Hirvonen, et al., Differential expression of myc, max and RB1 genes in human gliomas and glioma cell lines, Br. J. Cancer 69 (1) (1994) 16–25.
[72] S.H. Bigner, et al., Relationship between gene amplification and chromosomal deviations in malignant human gliomas, Cancer Genet. Cytogenet. 29 (1) (1987) 165–170.
[73] A.M. Stenger, et al., N-myc oncogene amplification in a pediatric case of glioblastoma multiforme, Childs Nerv. Syst. 7 (7) (1991) 410–413.
[74] A. Asai, et al., Negative effects of wild-type p53 and s-Myc on cellular growth and tumorigenicity of glioma cells Implication of the tumor suppressor genes for gene therapy, J. Neurooncol. 19 (3) (1994) 259–268.
[75] C.L. Appin, D.J. Brat, Molecular pathways in gliomagenesis and their relevance to neuropathologic diagnosis, Adv. Anat. Pathol. 22 (1) (2015) 50–58.
[76] B.K. Rasheed, et al., Alterations of the TP53 gene in human gliomas, Cancer Res. 54 (5) (1994) 1324–1330.
[77] D.J. van Meyel, et al., p53 mutation, expression, and DNA ploidy in evolving gliomas: evidence for two pathways of progression, J. Natl. Cancer Inst. 86 (13) (1994) 1011–1017.
[78] S. Yamasaki, et al., The roles of synoviolin in crosstalk between endoplasmic reticulum stress-induced apoptosis and p53 pathway, Cell Cycle 6 (11) (2007) 1319–1323.
[79] J. He, L.G. Baum, Presentation of galectin-1 by extracellular matrix triggers T cell death, J. Biol. Chem. 279 (6) (2004) 4705–4712.
[80] L.G. Toussaint, 3rd, et al., Galectin-1, a gene preferentially expressed at the tumor margin, promotes glioblastoma cell invasion, Mol. Cancer 11 (2012) 32.
[81] T. Verschuere, et al., Glioma-derived galectin-1 regulates innate and adaptive antitumor immunity, Int. J. Cancer 134 (4) (2014) 873–884.
[82] D. Tang, et al., High expression of Galectin-1 in pancreatic stellate cells plays a role in the development and maintenance of an immunosuppressive microenvironment in pancreatic cancer, Int. J. Cancer 130 (10) (2012) 2337–2348.
[83] K. Ma, et al., DNA methylation-regulated miR-193a-3p dictates resistance of hepatocellular carcinoma to 5-fluorouracil via repression of SRSF2 expression, J. Biol. Chem. 287 (8) (2012) 5639–5649.
[84] L. Lv, et al., The DNA methylation-regulated miR-193a-3p dictates the multi-chemoresistance of bladder cancer via repression of SRSF2/PLAU/HIC2 expression, Cell Death Dis. 5 (2014) e1402.
[85] L. Lv, et al., MiR-193a-3p promotes the multi-chemoresistance of bladder cancer by targeting the HOXC9 gene, Cancer Lett. 357 (1) (2015) 105–113.
[86] R. Agrawal, et al., Hypoxic signature of microRNAs in glioblastoma: insights from small RNA deep sequencing, BMC Genomics 15 (2014) 686.
[87] V. Edmond, et al., Acetylation and phosphorylation of SRSF2 control cell fate decision in response to cisplatin, EMBO J. 30 (3) (2011) 510–523.
[88] S.W. Jang, et al., Interaction of Akt-phosphorylated SRPK2 with 14-3-3 mediates cell cycle and cell death in neurons, J. Biol. Chem. 284 (36) (2009) 24512–24525.